IIB 2010

Inverse temperature dependence of activation volume in ultrafine-grained copper processed by accumulative roll-bonding

Takahiro Kunimine · Takashi Aragaki · Toshiyuki Fujii · Susumu Onaka · Masaharu Kato

Abstract Tensile tests and strain-rate jump tests were carried out at several temperatures below room temperature on Cu processed by accumulative roll-bonding (ARB). The temperature dependences of the flow stress and the activation volume were determined. In contrast to conventional coarse-grained materials where the activation volume increases with increasing temperature, the ARB processed copper by 8 cycles with ultrafine-grains showed inverse temperature dependence of activation volume, i.e., decreased activation volume with increasing temperature. This inverse temperature dependence of the activation volume is discussed in terms of thermally activated dislocation bow-out from grain-boundaries.

Introduction

High-strength metallic materials have been produced for decades by severe plastic deformation (SPD) such as accumulative roll-bonding (ARB), equal channel angular pressing (ECAP), and high pressure torsion (HPT) [1–5]. Microstructural evolution in FCC metals and alloys during SPD has been extensively investigated [6–10]. Following the formation of a deformation structure consisting of high-density dislocations and subgrain boundaries [9], ultrafine-grains (UFGs) smaller than about 1 μm and surrounded by high-angle grain boundaries appear during SPD. The new UFGs coexist with the deformation structure in SPD processed metals and alloys [6–8].

It has been shown that SPD processed materials with UFGs have some characteristic mechanical properties that are different from those of their coarse-grained (CG) counterparts [11, 12]. The characteristic mechanical properties observed in the SPD processed materials are fairly similar to those of nanocrystalline (NC) materials [13, 14]. Although several unique phenomena have been reported for mechanical properties of SPD processed materials, the controlling mechanisms of these phenomena are not well understood. This study focuses on a unique phenomenon in the mechanical properties of the SPD processed materials, namely the inverse temperature dependence of the activation volume of plastic deformation.

The temperature T dependence of the activation volume V^* for single crystals (SC) and CG polycrystals of FCC metals has been reported [15, 16]. For example, Conrad has discussed the temperature dependence of V^* at certain amounts of plastic strain ε for SC and CG polycrystals of copper and aluminum [15]. It was shown that at temperatures below room temperature (RT) V^* at constant ε increases with increasing T [15]. Bochniak [16] reported the temperature dependence of V^* as a function of the flow stress σ for SC copper, aluminum and silver. Comparison of the results at 77 K and RT shows that (i) V^* at constant σ increases with increasing T, and (ii) V^* at constant T decreases with increasing σ [16]. Since σ at constant ε decreases with increasing T, the results obtained by Bochniak imply that V^* at constant ε increases with increasing T. As shown in the studies by Conrad [15] and Bochniak [16], increase of V^* with increasing T is the usual relationship between V^* and T for SC and CG polycrystals

T. Kunimine (✉) · T. Aragaki · S. Onaka · M. Kato
Department of Materials Science and Engineering, Tokyo Institute of Technology, 4259 Nagatsuta-cho, Midori-ku, Yokohama 226-8502, Japan
e-mail: kuniminet9@gmail.com

T. Fujii
Department of Innovative and Engineered Materials, Tokyo Institute of Technology, 4259 Nagatsuta-cho, Midori-ku, Yokohama 226-8502, Japan

of FCC metals. This relationship has been explained by the deformation mechanism considering the interaction between dislocations and obstacles in grains [11].

In recent studies on FCC metals with grains in the range 10 nm to 1 μm [13, 17, 18], it has been reported that the activation volume decreases with increasing temperature at temperatures below RT. The same temperature dependence of $V*$ has also been reported for SPD processed FCC metals [11]. Such a temperature dependence of $V*$ is quite different from that for the SC and CG metals. This unique phenomenon, the decrease of $V*$ with increasing T, is referred to hereinafter as the inverse temperature dependence of the activation volume and suggests a rate-controlling mechanism that is common to the NC, UFG (ultrafine-grained) and SPD-processed metals. In conventional materials with coarse grains larger than about 1 μm, in-grain dislocation sources operate, whereas for NC and UFG materials it is reported that dislocation sources in grain boundaries control the motion of dislocations [19–21].

As a deformation mechanism in NC and UFG metals, emission and bow-out of grain-boundary dislocations has been proposed [20, 21]. Using the dislocation bow-out model, Kato [21] has analyzed quantitatively the inverse temperature dependence of $V*$ for NC Ni. Using experimental results for NC Ni from previous studies, Kato assigned activation parameters that reasonably explain the temperature dependence of the effective stress [21]. Using these activation parameters, Kato compared the experimental results with theoretical calculations for the temperature dependence of $V*$ for NC Ni and established the validity of the dislocation bow-out model [21].

In this study, the inverse temperature T dependence of the activation volume $V*$ is discussed for SPD processed copper, and experimental results are analyzed with the dislocation bow-out model [21]. However, in a departure from Kato's analysis [21], comparison of the experimental with the theoretical results is made without assigning activation parameters. The authors thus demonstrate the validity of the dislocation bow-out model using a different approach from that adopted by Kato [21].

Experimental procedure

Polycrystalline copper sheets of 99.99% purity were used as a primary material. After annealing at 873 K for 2 h, the copper sheets were subjected to ARB for up to 8 cycles (8C) at RT. The ARB process is a technique for grain refinement by rolling deformation [22, 23]. Tensile specimens were cut from the copper sheets of 8C with an electro discharge machine. The average width of high-angle lamellar boundaries of grains in the specimens was about

370 nm. Many dislocations were observed in these specimens; however, UFGs with lower dislocation density in the deformation structure were also observed. Tensile tests were performed with an Instron-type testing machine at various temperatures between 77 K and RT. The initial strain-rate $\dot{\varepsilon}_1$ of the tensile tests was $8.3 \times 10^{-5} \mathrm{s}^{-1}$. Strain-rate jump tests were conducted between $\dot{\varepsilon}_1 = 8.3 \times 10^{-5} \mathrm{s}^{-1}$ and $\dot{\varepsilon}_2 = 8.3 \times 10^{-4} \mathrm{s}^{-1}$. From measurements of the change in flow stress from σ_1 under $\dot{\varepsilon}_1$ to σ_2 under $\dot{\varepsilon}_2$, the activation volume $V*$ was evaluated from the equation

$$V^* = MkT\frac{\ln(\dot{\varepsilon}_2/\dot{\varepsilon}_1)}{\sigma_2 - \sigma_1}, \tag{1}$$

where k is the Boltzmann constant and $M = 3.06$ is the Taylor factor for FCC polycrystals.

Results and discussion

Inverse temperature dependence of activation volume

Figure 1 shows the temperature T dependence of the flow stress σ at plastic strain $\varepsilon \approx 0.01$ for the 8C specimens. The flow stresses for two kinds of strain rates are obtained by the strain-rate jump tests at $\varepsilon \approx 0.01$. The square symbols indicate the values of σ_1 under $\dot{\varepsilon}_1 = 8.3 \times 10^{-5} \mathrm{s}^{-1}$ and the diamond symbols indicate the values of σ_2 under $\dot{\varepsilon}_2 = 8.3 \times 10^{-4} \mathrm{s}^{-1}$. The values of σ_1 were about 600 MPa at 77 K and 435 MPa at RT. While both σ_1 and σ_2 decreased with increasing T, the difference $\Delta\sigma = \sigma_2 - \sigma_1$ increased with increasing T. At RT $\Delta\sigma$ was about 15 MPa.
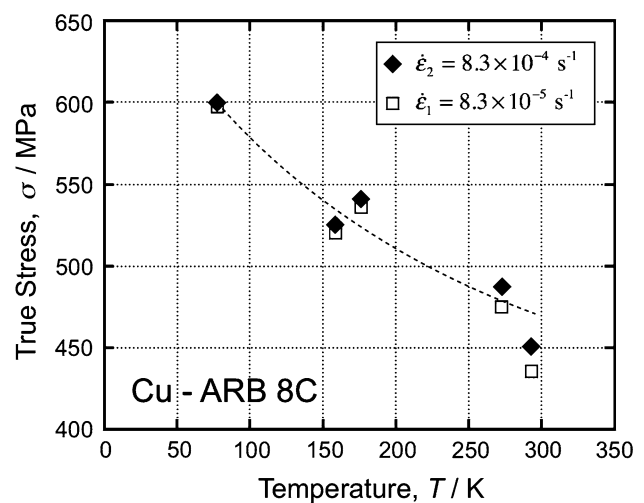

Fig. 1 Temperature T dependence of the flow stress σ at plastic strain $\varepsilon \approx 0.01$ for the copper specimens ARB processed by 8 cycles. The flow stresses for two kinds of strain-rates are obtained by the strain-rate jump tests at $\varepsilon \approx 0.01$

Using the relationship between $\Delta\sigma$ and T in Fig. 1, the authors can obtain the temperature T dependence of the activation volume V^* from Eq. 1. As shown in Fig. 2, the values of V^* were about $200b^3$ at 77 K and $130b^3$ at RT, where b is the magnitude of the Burgers vector. The overall trend of the temperature dependence of V^* in Fig. 2 is the decrease of V^* with increasing T, that is, the inverse temperature dependence of V^*.

Figure 3 shows the relationships between the flow stress σ and the activation volume V^* at RT for copper of various states. The open squares are data for CG polycrystalline copper [24], which show the variation of V^* during work hardening of the CG copper. The results for the CG copper are on a dotted line with a slope of -1 in Fig. 3, which means a proportional relation between σ and $1/V^*$. This σ–V^* relationship is explained by the Taylor equation when the rate-controlling deformation mechanism is cutting of forest dislocations by moving dislocations in the grain interior [11]. However, the proportional relation between σ and $1/V^*$ for the CG copper is not satisfied for NC and SPD copper, as indicated by the data for the nanotwin copper [25], the ARB processed copper by 8C (this study) and the ECAP processed copper by 16 passes [26]. The nanotwin copper has nanoscale twin boundaries and is one of the NC materials. The deviation from the proportional relation between σ and $1/V^*$ for the CG copper indicates a change in the dominant deformation mechanism from that related to the grain interior to that related to grain boundaries [11]. Although the deviation is most significant for the nanotwin copper, the rate-controlling mechanism may be similar for nanotwin and SPD copper.
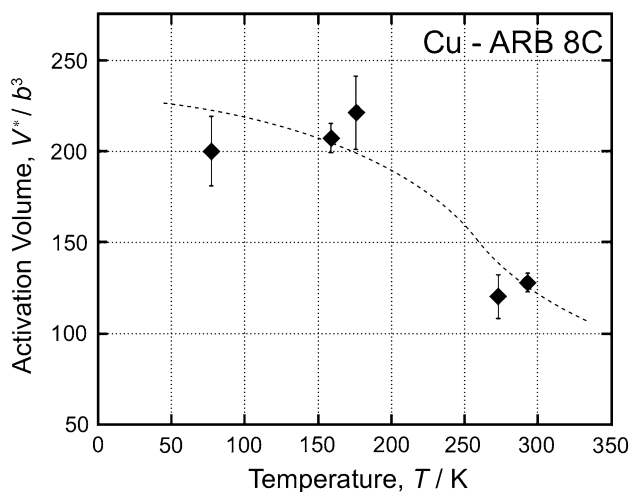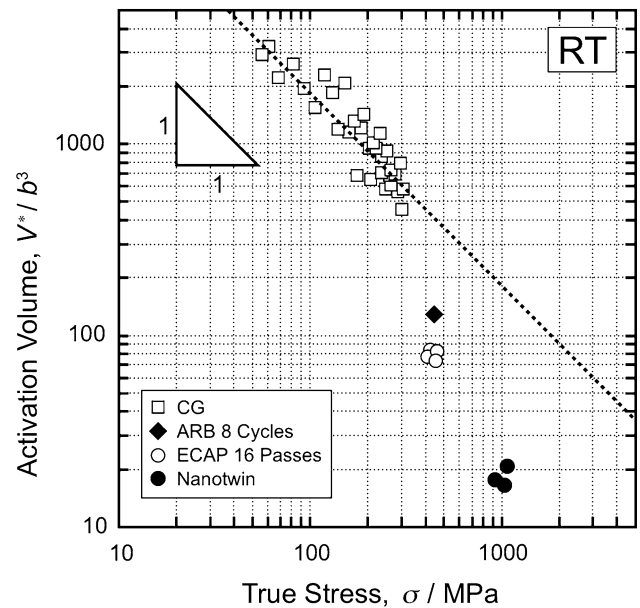

Fig. 3 The relationships between the flow stress σ and the activation volume V^* at RT for copper of various states, i.e., CG polycrystal [24], ARB by 8C (this study), ECAP by 16 passes [26] and nanotwin [25]. The data points for the nanotwin copper were converted from the values of the strain-rate sensitivity m in [25]

Thermally activated process in bow-out of dislocation emitted from grain-boundary source

As shown by the temperature and strain rate dependences of σ in Fig. 1, a thermally activated dislocation process is included in the plastic deformation of ARB processed copper. For UFG materials, it is regarded that plastic deformation occurs by motion of dislocations emitted from grain-boundary (GB) sources [19–21]. After bow-out of a dislocation between pinning points on GB, escape of the dislocation from GB determines the occurrence of plastic deformation [11, 20, 21]. The pinning points on GB are most probably short-range obstacles for the escape of the dislocation [11, 13, 20, 21]. In a previous study [27], absolutely strong GB pinning points that dislocations could not overcome by a thermally activated dislocation process were assumed. However, theoretical consideration on mechanical properties of NC materials based on this assumption failed to explain the experimental results obtained by various researchers [27].

Figure 4 shows the bow-out of the dislocation and the thermally activated depinning at one of the pinning points at (a) lower and (b) higher temperatures. In these figures, L_{GB} is the average distance between the GB pinning points and w^* the activation distance of the GB pinning point. The two curves in each figure are the shapes of the dislocation just before and after the thermally activated depinning. The dislocation shapes at depinning are in the equilibrium state with the same critical radius r. The critical angle θ is

Fig. 2 The relationship between the temperature T and the activation volume V^* at the plastic strain $\varepsilon \approx 0.01$ for the copper specimens ARB processed by 8 cycles

Fig. 4 The schematic illustration showing the shape of bowing-out dislocation emitted from grain-boundary source between pinning obstacles at **a** lower and **b** higher temperatures
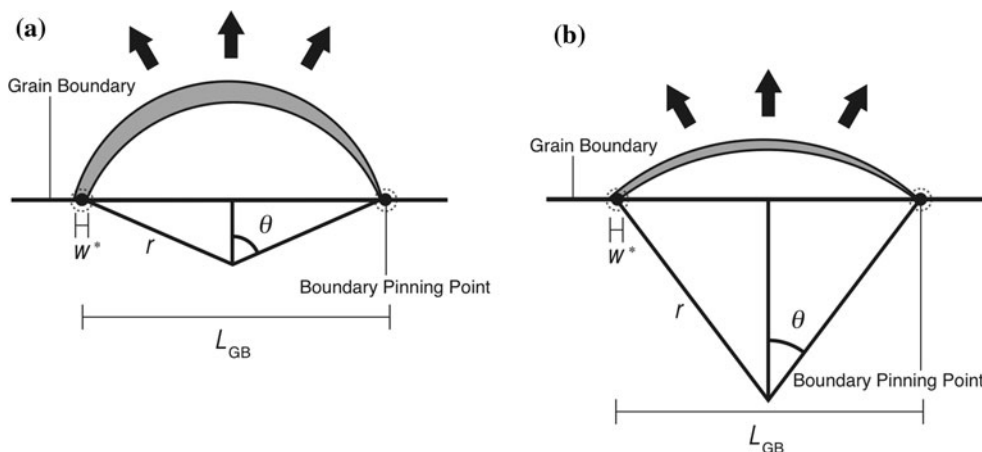
related to L_{GB} and r as $2r\sin\theta = L_{GB}$. The shaded area bounded by the two shapes of the dislocation is the activation area.

It is apparent that the dislocation bows out more at lower than at higher temperature, because depinning becomes easier with increasing temperature. Since the activation volume V^* is proportional to the activation area shown by the shaded area, the dislocation bow-out and depinning model can reasonably explain the inverse temperature dependence of V^* [11].

Relationship between activation volume and effective stress in the dislocation bow-out model

For the thermally activated dislocation process shown in Fig. 4, Kato [21] derived an expression for the activation volume V^* as a function of L_{GB}, w^*, r, and b:

$$V^* = r^2 b \left\{ \left[\sin^{-1}\left(\frac{L_{GB}+w^*}{2r}\right) - \left(\frac{L_{GB}+w^*}{2r}\right) \right. \right.$$
$$\left. \times \sqrt{1 - \left(\frac{L_{GB}+w^*}{2r}\right)^2} \right] - \left[\sin^{-1}\left(\frac{L_{GB}}{2r}\right) \right.$$
$$\left. \left. - \left(\frac{L_{GB}}{2r}\right)\sqrt{1 - \left(\frac{L_{GB}}{2r}\right)^2} \right] \right\}. \tag{2}$$

For UFG materials, the distance L_{GB} between the GB pinning points is estimated to be about one-third of the grain size [20]. On the other hand, the activation distance w^* is estimated to be in the order of b. Therefore, $L_{GB} \gg w^*$ is satisfied for UFG materials with the grain size in the range 10 nm $\sim$ 1μm. In this case, the critical angle θ satisfying $2r\sin\theta = L_{GB}$ becomes smaller than about 1 radian and the activation volume V^* given by Eq. 2 is written approximately as

$$V^* \approx \frac{1}{2}L_{GB}w^*b\sin\theta\left(1 + \frac{\sin^2\theta}{2}\right). \tag{3}$$

The derivation of Eq. 3 is shown in the Appendix.

The bow-out of a dislocation is caused by stress acting on the dislocation. In general, the shear flow stress τ has two components, i.e.,

$$\tau = \tau^* + \tau_a, \tag{4}$$

where τ^* is the effective stress and τ_a the athermal stress. The effective stress τ^* controls thermally activated depinning and determines the critical angle θ. Considering the equilibrium between forces acting on a dislocation, τ^* is written as

$$\tau^* b L_{GB} = 2T_L \sin\theta, \tag{5}$$

where T_L is the line tension of dislocation given by

$$T_L = \alpha\mu b^2. \tag{6}$$

Here, μ is the shear modulus and α is taken to be 0.5 in this study. From Eqs. 3, 5, and 6, the activation volume V^* is written as a function of τ^* as

$$V^* \approx \frac{\tau^* w^* L_{GB}^2}{2\mu}\left(1 + \frac{\tau^{*2}L_{GB}^2}{2\mu^2 b^2}\right). \tag{7}$$

Since τ^* decreases with increasing T, Eq. 7 naturally shows the decrease in V^* with increasing T, i.e., the inverse temperature dependence of V^*.

Effective stress and athermal stress of ARB processed copper

Let us now evaluate the temperature dependence of τ^* with Eq. 7 using the experimental results in Fig. 2. From this evaluation, the validity of the dislocation bow-out model can be examined by comparing the evaluated temperature dependence of τ^* to the experimental results on the temperature dependence of the flow stress σ shown in Fig. 1.

The average distance L_{GB} between the pinning points has been estimated by a statistical consideration by Kato et al. [20] as

$$L_{GB} = (d + 2\lambda)/3, \tag{8}$$

where d is the grain size and λ the minimum distance between the pinning points on GB. The value of λ is estimated to be about 10 nm in FCC metals [20, 21]. Since the grain size d of the ARB processed copper by 8C is about 370 nm, L_{GB} for the 8C copper is about 130 nm. Using $L_{GB} = 130$ nm and assuming $w^* = b$, the authors have evaluate the temperature dependence of τ^* from the results shown in Fig. 2. Here, materials constants for copper, $b = 0.25$ nm and

$$\mu = 42.1 \times \left[1 - (T - 300) \times 3.97 \times 10^{-4}\right] (\text{GPa}) \tag{9}$$

are used [28]. In these calculations, the condition $\theta < 1$ was satisfied so that the approximation of Eq. 3 was valid. To compare the shear effective stress τ^* obtained by the calculations with the tensile flow stress σ shown in Fig. 1, using the Taylor factor $M = 3.06$, the authors have obtained the tensile effective stress σ^* given by

$$\sigma^* = M\tau^*. \tag{10}$$

By evaluating σ^* from V^* at various temperatures, the authors can decompose the tensile flow stress σ into the two components, the tensile effective stress σ^* and the athermal stress σ_a. Figure 5 shows the values of σ^* and σ_a at various T. As shown in Fig. 5, the athermal stress σ_a at various temperatures is nearly the same, as should be the case. Furthermore, it can be seen from Fig. 5 that the fraction of the effective stress σ^* in σ is about 0.25 at RT. This value is almost the same as the ratio $\sigma^*/\sigma \approx 0.17$ given by stress relaxation tests of ECAP processed copper [26]. These show that the dislocation bow-out model
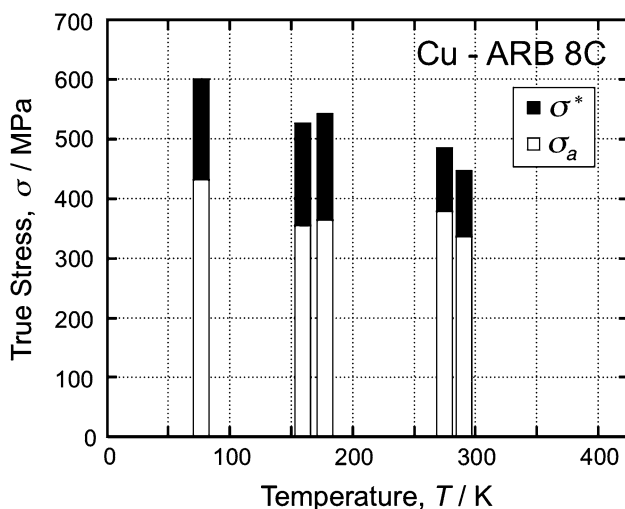
Fig. 5 The effective stress σ^* and the athermal stress σ_a in the flow stress σ as a function of temperature T. The effective stress σ^* is evaluated from experimental results of V^* by using the dislocation bow-out model. See text for details of the calculations

results in the reasonable evaluation of σ^* from V^* and well explains the deformation behavior in the ARB processed copper by 8C.

The microstructure of ARB processed copper changes from deformation structure to UFG structure with increasing number of ARB cycles. In the ARB processed copper by 8C, UFGs coexisted with the deformation structure. These results have provided evidence that the rate-controlling deformation mechanism of SPD Cu is dislocation bow-out from grain-boundaries of UFGs.

Summary

An attempt has been made to explain the inverse temperature dependence of the activation volume for ARB processed copper by 8C. From the experimental results on the temperature T dependence of the activation volume V^*, the temperature dependence of the effective stress σ^* has been evaluated from the dislocation bow-out model. The authors have found that the evaluated temperature dependence of σ^* reasonably explains the experimentally determined temperature dependence of the flow stress σ in the ARB processed copper by 8C. Although ultrafine-grains coexist with deformation structure in SPD processed copper, these results have shown that the rate-controlling deformation mechanism is the dislocation bow-out from grain-boundaries.

Appendix. Derivation of Eq. 3 from Eq. 2

Eq. 2 can be rewritten as

$$V^*/(r^2 b) = \left[\sin^{-1}(\eta + \delta\eta) - \sin^{-1}(\eta)\right] \\ - \left[(\eta + \delta\eta)\sqrt{1 - (\eta + \delta\eta)^2} - \eta\sqrt{1 - \eta^2}\right], \tag{11}$$

where $\eta = L_{GB}/(2r) > 0$ and $\delta\eta = w^*/(2r) > 0$. The authors also have $\eta = L_{GB}/(2r) = \sin\theta$ where θ is the critical bow-out angle. Since the activation distance w^* of the pinning point is naturally much shorter than the average distance L_{GB} between pinning points, the authors have $|\delta\eta/\eta| \ll 1$.

The function $\sin^{-1}(\eta)$ in the right side of Eq. 11 is given by the series written as

$$\sin^{-1}(\eta) = \sum_{n=0}^{\infty} \frac{(2n-1)!!\,\eta^{2n+1}}{(2n)!!(2n+1)}, \tag{12}$$

where $(2n-1)!! = (2n-1)(2n-3)\dots 3\cdot 1$ and $(2n)!! = (2n)(2n-2)\dots 4\cdot 2$. When $|\delta\eta/\eta| \ll 1$, we have

$$
\begin{aligned}
\sin^{-1}(\eta+\delta\eta) &= \sum_{n=0}^{\infty} \frac{(2n-1)!!(\eta+\delta\eta)^{2n+1}}{(2n)!!(2n+1)} \\
&\approx \sum_{n=0}^{\infty} \frac{(2n-1)!![\eta^{2n+1}+(2n+1)\eta^{2n}\delta\eta]}{(2n)!!(2n+1)}.
\end{aligned}
\tag{13}
$$

From Eqs. 12 and 13, we have

$$\left[\sin^{-1}(\eta+\delta\eta) - \sin^{-1}(\eta)\right] \approx \sum_{n=0}^{\infty} \frac{(2n-1)!!\,\eta^{2n}\delta\eta}{(2n)!!}. \tag{14}$$

When θ is not so large, for example, $\theta < 1$, the higher-order terms of η^{2n}, such as η^6, η^8, η^{10},…, can be regarded much smaller than $\eta^0 = 1$. Hence, we have

$$\left[\sin^{-1}(\eta+\delta\eta) - \sin^{-1}(\eta)\right] \approx \delta\eta\left(1 + \frac{\eta^2}{2} + \frac{3\eta^4}{8}\right). \tag{15}$$

When $0 < \delta\eta/\eta \ll 1$ is satisfied and the higher-order terms of η^{2n} are neglected, we also have

$$
\begin{aligned}
&\left[(\eta+\delta\eta)\sqrt{1-(\eta+\delta\eta)^2} - \eta\sqrt{1-\eta^2}\right] \\
&\approx \delta\eta\left(1 - \frac{3\eta^2}{2} - \frac{5\eta^4}{8}\right).
\end{aligned}
\tag{16}
$$

From Eqs. 11, 15 and 16, the authors have

$$V^*/(r^2 b) \approx \delta\eta\left(2\eta^2 + \eta^4\right). \tag{17}$$

Using $\eta = L_{GB}/(2r)$, $\delta\eta = w^*/(2r)$ and $r = L_{GB}/(2\sin\theta)$, Eq. 3 can be obtained from Eq. 17.

References

1. Meyers MA, Mishra A, Benson DJ (2006) Prog Mater Sci 51:427–556
2. Azushima A, Kopp R, Korhonen A, Yang DY, Micari F, Lahoti GD, Groche P, Yanagimoto J, Tsuji N, Rosochowski A, Yanagida A (2008) CIRP Ann-Manuf Technol 57:716–735
3. Valiev RZ (2007) J Mater Sci 42:1483–1490. doi:10.1007/s10853-006-1281-3
4. Zhilyaev AP, McNelley TR, Langdon TG (2007) J Mater Sci 42:1517–1528. doi:10.1007/s10853-006-0628-0
5. Langdon TG (2007) J Mater Sci 42:3388–3397. doi:10.1007/s10853-006-1475-8
6. Mishra A, Richard V, Gregori F, Asaro RJ, Meyers MA (2005) Mater Sci Eng A 410–411:290–298
7. Takata N, Yamada K, Ikeda K, Yoshida F, Nakashima H, Tsuji N (2007) Mater Trans 48:2043–2048
8. Edalati K, Fujioka T, Horita Z (2008) Mater Sci Eng A 497:168–173
9. Ito Y, Horita Z (2009) Mater Sci Eng A 503:32–36
10. Hanazaki K, Shigeiri N, Tsuji N (2010) Mater Sci Eng A 527:5699–5707
11. Kunimine T, Takata N, Tsuji N, Fujii T, Kato M, Onaka S (2009) Mater Trans 50:64–69
12. Huang X, Hansen N, Tsuji N (2006) Science 312:249–251
13. Wang YM, Hamza AV, Ma E (2006) Acta Mater 54:2715–2726
14. Wang YM, Cheng S, Wei QM, Ma E, Nieh TG, Hamza A (2004) Scr Mater 51:1023–1028
15. Conrad H (1965) In: Zackay VF (ed) High-Strength Materials. John Wiley & Sons, Inc, New York
16. Bochniak W (1995) Acta Metall Mater 43:225–233
17. Conrad H, Yang D (2002) J Electron Mater 31:304–312
18. Conrad H (2003) Mater Sci Eng A 341:216–228
19. Cheng S, Spencer JA, Milligan WW (2003) Acta Mater 51:4505–4518
20. Kato M, Fujii T, Onaka S (2008) Mater Trans 49:1278–1283
21. Kato M (2009) Mater Sci Eng A 516:276–282
22. Tsuji N, Saito Y, Utsunomiya H, Tanigawa S (1999) Scr Mater 40:795–800
23. Tsuji N (2006) In: Altan BS, Miskioglu I, Purcek G, Mulyukov RR, Artan R (eds) Severe plastic deformation: towards bulk production of nanostructured materials. NOVA Science Publishers, New York
24. Kunimine T, Fujii T, Onaka S, Tsuji N, Kato M, in press
25. Shen YF, Lu L, Dao M, Suresh S (2006) Scr Mater 55:319–322
26. Dalla Torre FH, Pereloma EV, Davies CHJ (2006) Acta Mater 54:1135–1146
27. Estrin Y, Kim HS, Nabarro FRN (2007) Acta Mater 55:6401–6407
28. Frost HJ, Ashby MF (1982) Deformation-Mechanism Maps. Pergamon, Oxford